Fuel 90 (2011) 2760–2766

Contents lists available at ScienceDirect

Fuel

journal homepage: www.elsevier.com/locate/fuel

Influence of low air pressure on combustion characteristics and flame pulsation frequency of pool fires

Jun Fang *, Ran Tu, Jin-fu Guan, Jin-jun Wang, Yong-ming Zhang

State Key Laboratory of Fire Science, University of Science and Technology of China, Hefei, Anhui 230026, PR China

ARTICLE INFO

Article history:
Received 25 January 2011
Received in revised form 25 March 2011
Accepted 25 March 2011
Available online 8 April 2011

Keywords:
Pool fire
Buoyancy effect
Combustion characteristics
Flame oscillation frequency
Low air pressure

ABSTRACT

To investigate the effect of low air pressure on the combustion characteristics and puffing flame frequency of pool fires, ethanol and *n*-heptane pool fires were performed using 15 square burners of various size in both Lhasa (altitude: 3650 m; air pressure: 65 kPa) and Hefei (altitude: 24 m, air pressure: 100.8 kPa) fire laboratories. Comparison of the experimental results for pool fires of the same size in the two places shows that, firstly, the maximum rise in the centerline temperature in flames in Lhasa is generally larger than that in Hefei. Secondly, the dependence of the burning rate exponent n ($\dot{m}'' \propto p^n$) on the air pressure varies with the equivalent diameter D of the burner, with $n < 0$ ($D < 7$ cm), (0–1) (7 cm < D < 10 cm), (1–1.45) (10 cm < D < 19 cm) and 1 ($D > 19$ cm). Thirdly, radiation fraction of the pool fire flames is smaller at low air pressure. Finally, the puffing frequency of the pool fire flames is higher at low air pressure. Compared with Hefei, in Lhasa, for the same size burner, a higher maximum temperature together with less radiation from the flame is observed. This shows that in low air pressure, the pool fire is more buoyant, which leads to stronger periodic oscillation and a higher flame puffing frequency.

1. Introduction

Pool fires and buoyant diffusion flames are major elements in the development of many unwanted fires. These flames exhibit a periodic oscillatory movement that is often referred to as 'puffing' or 'flickering'. In a fire, these oscillations are associated with the formation of flaming vortical structures; the frequency of the toroidal vortices correlates with the flame oscillation frequency, which mainly depends on the burner diameter with the relation $f \propto D^{-1/2}$ [1–3].

In the investigation of air pressure effects upon fire frequency, many available studies have been limited to the effects of pressure upon diffusion flames, focusing on soot and temperature profiles at elevated pressures [4,5]. The study of flame flicker under elevated air pressure has attracted some attention, while that under low air pressure is scarce. Of the research published on the effect of low air pressure upon diffusion flames [6–8], most studies used a gas–air co-flow diffusion flame in a small confined chamber. The pressure and co-flow were controlled independently, and the oscillation frequency was reported to be proportional to the air pressure. For a laminar jet flame, the relationship between puffing frequency and pressure is $f \propto (p^2 g)^{1/3}$. In these studies, the experimental chambers were relatively small, so some confining effects might affect the results. Therefore, the results from co-flow laminar jet flame studies are unable to provide guidance for prevention of actual highland fires.

In Lhasa, capital of Tibet Autonomous Region of China, the average altitude is 3650 m, and the air pressure and oxygen content are about only 2/3 of those in the plain areas. In recent years, a fire laboratory has been constructed in Lhasa, and a series of experiments on the combustion characteristics and fire products under low ambient air pressure conditions have been investigated. Li et al. [9] performed a preliminary study of *n*-heptane pool fires and wood crib fires; burning rates, centerline temperature, and radiation heat flux were analyzed using the same size burner and burning rate in Lhasa and Hefei. Fang et al. [10] studied the influence of low air pressure upon CO products from *n*-heptane pool fires in a confined test room. To date, the effect of burner size upon flame characteristics and flame pulsation frequency at low pressure has not been studied.

In this work, liquid pool fires were studied in fire laboratories in Lhasa and Hefei. Unlike previous studies of controlled co-flow jet diffusion flames, in Lhasa both the air pressure and oxygen density decrease in a natural manner. This leads to natural changes in the flame temperature, radiation and puffing frequency. The objective was to investigate the influence of low air pressure on laminar/transitional buoyant diffusion flame dynamics of pool fires. This was achieved by performing fire tests using 15 square burners of various sizes at low and high altitude with two kinds of fuels, providing scientific support for fire prevention and detection in high altitude areas.

* Corresponding author. Tel.: +86 551 3607119; fax: +86 551 3601669.
E-mail address: fangjun@ustc.edu.cn (J. Fang).

0016-2361/$ - see front matter © 2011 Elsevier Ltd. All rights reserved.
doi:10.1016/j.fuel.2011.03.035

Nomenclature

p	air pressure (kPa)
$\dot{m}''$	burning rate (g cm^{-2} s^{-1})
n	exponent for burning rate dependence upon air pressure ($\dot{m}'' \propto p^n$)
f	flame oscillation frequency (Hz)
z	vertical height (cm)
λ	thermal conductivity (W m^{-1} K^{-1})
h	convection heat transfer coefficient (W m^{-2} K^{-1})
ε	surface emissivity
σ	Stefan–Boltzmann constant (W m^{-2} K^{-4})
κ_s	absorption coefficient (m^{-1})
L, D	square burner inner side, equivalent burner inner diameter (cm, m)
A	burner surface area (cm^2)
M	molecular weight (kg mol^{-1})
R	universal gas constant (8.3145 J mol^{-1} K^{-1})
T	mean temperature (K, °C)
$\dot{Q}$	heat release rate (kW)
$\dot{q}''_r$, $\dot{Q}_r$	radiant heat flux (kW m^{-2}), radiant heat (kW)
ΔH_c	enthalpy of combustion (kJ g^{-1})
ΔT ($T_f - T_\infty$)	mean flame gas temperature rise above ambient (K, °C)
S_r	flame radiant area (cm^2)
T_l, T_f	liquid boiling temperature, flame gas temperature (K, °C)
U_l, U_{f0}	liquid regression rate, vapor velocity at source (cm s^{-1})
ρ_l, ρ_{f0}, ρ_f	liquid density at source, vapor density at source, hot mixing gas density in flame (g cm^{-3})
χ_r	radiant fraction of heat release rate
Fr, Ri, Nu, Re, Pr	Froude number, Richardson number, Nusselt number, Reynolds number, Prandtl number

2. Theoretical analysis

Experimental studies indicate that three main zones can be identified in a pool fire flame as shown in the right upper part of Fig. 1. The flame puffing mechanism involves: acceleration of buoyant plume gas in stagnant surroundings resulting in formation of a toroidal vortical structure within one burner diameter above the surface, the decaying influence of the toroidal structure on the flame surface near the burner lip as it convects upward, and the accumulation of buoyant gas inside the flame envelope and its buoyant acceleration to form the next vortical structure [2].

To account for the change in oscillation frequency that occurs in low air pressure, a theoretical equation incorporating the Richardson number, buoyancy factor and burner size was used [1], as shown in the following equation:

$$f = K\sqrt{\frac{g}{D}}\left[\left(1+\frac{1}{Ri}\right)^{1/2} - \frac{1}{\sqrt{Ri}}\right]^{-1} \tag{1}$$

Here $K = C(\frac{\rho_\infty}{\rho_f} - 1)^{1/2}$, where C is a proportionality factor ranging between 0 and 1; the value of K is suggested to be approximately 0.5 according to experimental data [1]. The Richardson number is the ratio of buoyancy force and inertia force, $Ri = \frac{(\rho_\infty - \rho_f)gD}{\rho_f U_{f0}^2}$, while the Froude number is $Fr = \frac{U_{f0}^2}{gD}$.

Substituting K and Ri into Eq. (1), it can be rewritten as:

$$f = C\frac{U_{f0}}{D}(\sqrt{Ri+1}+1) \tag{2}$$

When $Ri \to \infty$, Eq. (2) can be simplified to Eq. (3).

$$f = C\sqrt{g}\sqrt{\frac{\rho_\infty - \rho_f}{\rho_f}}\frac{1}{\sqrt{D}} \tag{3}$$

Eq. (3) shows that buoyancy plays an important role in the puffing motion of a fire flame.

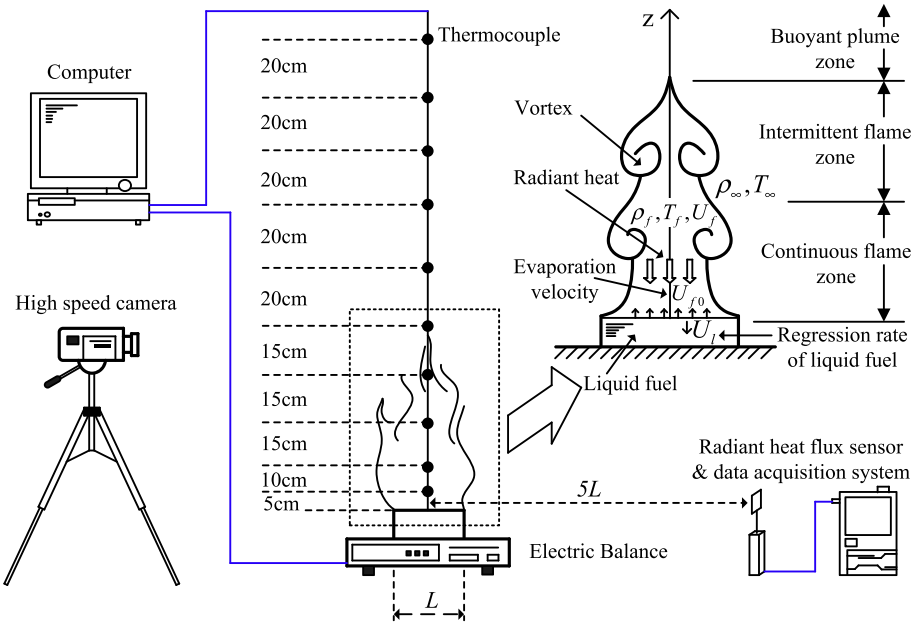

Fig. 1. Experimental setup for pool fire study.

3. Experimental systems

A schematic diagram of the experimental setup is shown in Fig. 1. The experiments were conducted in standard fire test rooms that were 10 m long, 7 m wide and 4 m high [10,11] in both Lhasa and Hefei. As proved by Hottel et al. [12,13], conduction from the flame to the burner rim is dominant for pool fire burning rate of pool diameters less than 7 cm, when diameter is bigger than 20 cm, burning rate becomes dominated by flame radiation. Finally the burning rate tends to level off for larger diameters. So in our work, fifteen steel square burners of various size (L = 4, 6, 7, 8, 9, 10, 11, 12, 13, 14, 17, 20, 24, 27, and 33 cm) with a thickness of 3 mm and a depth of 4 cm were located in the center of the test room for use. The depth of liquid in each burner was 3 cm. Ethanol and *n*-heptane were selected as fuel in consideration of the different sooty characteristics of their flames.

In Lhasa and Hefei, the ambient conditions were well-controlled so the variation in air pressure was less than 1 kPa in both locations. Except for air pressure, similar ambient temperature and humidity were used as much as possible in the two locations (Lhasa:20 °C, 50%; Hefei: 22 °C, 60%). The physical parameters of the liquid and vapor of ethanol and *n*-heptane in Lhasa and Hefei are shown in Table 1, where the vapor density was calculated from $\rho = pM/RT$.

In the experiments, data for the mass loss, axial temperature, radiation heat flux and flame video were recorded. The resolution of the electric balance was 0.1 g. A rack of ten armored K-type thermocouples with diameters of 1 mm was suspended above the burner surface in the centerline of the burner to measure the axial temperature of the pool fire. The thermocouples were coated with a stainless steel sheath to reduce the effect of radiation; their measurement range was between 0 and 1000 °C in 0.5 °C increments. In the experiments, the measured temperature value mainly reflects the flame gas temperature. A commercial radiant flux sensor (Captec, TS-30) with dimensions of 3×3 cm was placed at the same vertical position as the burner, horizontally away from the pool center by a distance of five times the size of the pool so that it was open to the flame radiation. The sensitivity of the sensor is 1.5 W/m^2 and the flux data was recorded by a DaqPRO-5300 acquisition system operating at a rate of one sample per second. For recording detailed flame images, a high speed camera (TroubleShooter 250) acquired images at a rate of 250 frames per second. Each test was repeated at least four times to ensure reproducibility of results.

4. Results and discussion

Pool fire growth is characteristic of initial accelerating period, developed period and extinction period. For liquid pool fire, the initial accelerating and extinction duration are very small. So firstly, in the experiments, the total mass decreases in two different linear regions, with slow and fast burning rates. In the fully developed period with a faster burning rate, the radiation flux, which is proportional to burning rate, fluctuates but remains near a maximum value for some time. The ethanol fires remain at maximum radiation flux for a longer time than *n*-heptane fires. Secondly, except for 4 cm side pool fires, in Lhasa, the fourteen ethanol and *n*-heptane pool fires with 6–33 cm sides possess smaller burning rates and radiation fluxes, leading to longer combustion time. For the fire with 4 cm sides, in Lhasa, the burning rate and radiation flux were abnormally large, especially in the fully developed period, so the combustion time in Lhasa is shorter than that in Hefei.

In the following discussion, all comparisons are based on the experimental results obtained in the stable zone during the fully developed combustion period, which was determined as the region where the burning rate approached the maximum value. Specifically, for each test, time-sequence burning rate data over a certain period were first selected. In the selected period, the burning rate data array included the maximum value and the smallest variance. The stable developed duration time varies among the different size burners, but is less than 60 s, which is long enough for subsequent temperature, radiation and flame image analysis. Secondly, the burning rate within the selected time was time-averaged. Thirdly, for repeatability, the burning rate used for final analysis was the average value for the repeat tests. Fluctuating temperature and radiation data were first smoothed using a smoothing algorithm, and then the data from the same stable period was averaged.

The experimental error in the burning rate for the 15 burners of different size was about 1–3% for the ethanol pool fire tests and about 2–5% for the *n*-heptane tests. The difference in burning rate between Lhasa and Hefei divided by the burning rate was about 15–55%. The experimental error in the flame temperature was about 5%, while the maximum difference in the flame temperature between the two places was about 10–30%.

4.1. Effects on the axial temperature, burning rate and radiation

4.1.1. Axial temperature

To consider the radiation effect upon the thermocouples, Luo's method [14] was used to correct the error of the measured temperature. As the radiation received from the flame is very small compared with the radiation the thermocouple gives off to the ambient, the error between actual flame temperature and measured thermocouple value is $\Delta T_{\text{error}} = T_f - T_{th} = \sigma\varepsilon_{th}(1-\varepsilon_f)T_f^4/(h + 4\sigma\varepsilon_{th}T_f^3)$, ΔT_{error} decreases with the decrease T_f. Here $h = \frac{Nu\cdot\lambda_g}{D_{th}} = \frac{\lambda_g}{D_{th}}[2 + (0.4\text{Re}^{0.5} + 0.06\text{Re}^{2/3})\text{Pr}^{0.4}]$[15] D_{th} is the thermocouple diameter, λ_g, Pr is mainly determined by the gas temperature, not influenced by air pressure except extremely high or low air pressure.

The change in the axial temperature ΔT (mean temperature rise above ambient) with $z/\dot{Q}^{2/5}$ for *n*-heptane and ethanol fires with sides of 4, 10, 20, and 27 cm in Lhasa and Hefei are shown in Fig. 2. Flame, intermittent and plume regions were identified based on the work of McCaffrey [16].

Interestingly, whether in Lhasa or in Hefei, the centerline temperatures of the *n*-heptane fires fall on the left side of ethanol fires in the horizontal axis. This is because *n*-heptane fires have larger enthalpy of combustion than ethanol fires. In addition, in Lhasa, the pool fire with 4 cm sides has a faster burning rate and a higher

Table 1
Liquid and vapor parameters for ethanol and *n*-heptane in Lhasa and Hefei.

Fuel material	Molecular formula	Liquid parameters (Lhasa, Hefei)				Vapor parameters (Lhasa, Hefei)
		Density (g cm^{-3})	Boiling point (°C)	Latent heat (kJ kg^{-1})	Enthalpy of combustion (MJ kg^{-1})	Density (g cm^{-3})
Ethanol	C_2H_6O	0.789, 0.789	67.0, 78.3	838, 838	29.7, 29.7	0.00108, 0.00157
n-heptane	C_7H_{16}	0.680, 0.680	89.0, 98.5	318, 318	48.5, 48.5	0.00221, 0.00324

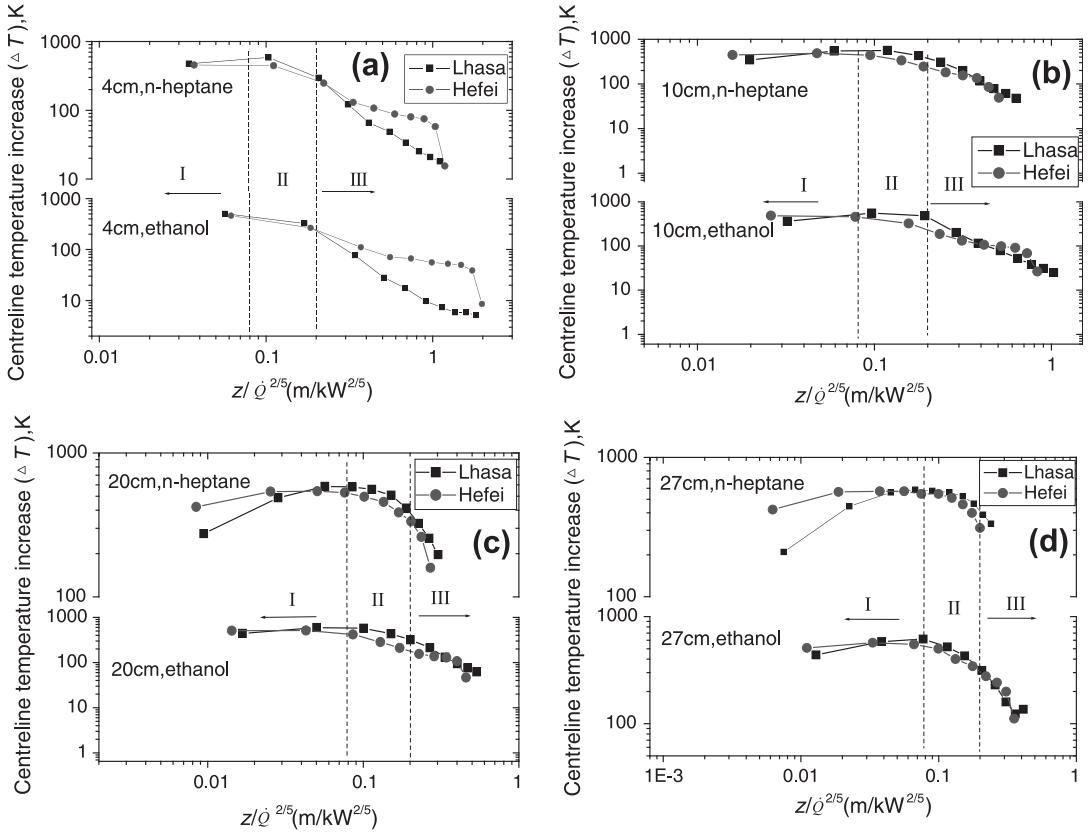

Fig. 2. Variation in the increase of centerline temperature with $z/\dot{Q}^{2/5}$ in ethanol and *n*-heptane pool fire flames in Lhasa and Hefei. The lengths of the burner sides were 4 cm (a), 10 cm (b), 20 cm (c) and 27 cm (d). Region I: flame region; Region II: intermittent zone; Region III: plume region.

rate of heat release, so the centerline temperature for both *n*-heptane and ethanol appears to the left of that in Hefei. For pool fires with sides longer than 4 cm, the burning rate in Lhasa is slower than that in Hefei. As a result, the rate of heat release decreases and the temperature data points shift to the right.

In the vertical axis, variations in temperature increase show different behavior. Firstly, near the burner surface, the axial flame temperature in Lhasa is lower than that in Hefei, the difference in temperature for the large pool fires reaches almost 200 K. This is because in the region near the burner surface the liquid is vaporized by combustion heat feedback, and the increase in flame temperature is mainly determined by rate of heat release from the fire. Because the pool fire with 4 cm sides in Lhasa and fires with bigger sides in Hefei have larger heat release, the temperature increase near the burner surface of the fire with 4 cm sides in Lhasa is higher than the same fire in Hefei; for fires with bigger sides, it is lower in Lhasa than in Hefei.

Secondly, as the height increases in the intermittent region, the temperature in Lhasa increases more quickly than in Hefei, leading to a larger increase in the maximum flame temperature in a very short length. The maximum temperature difference between Lhasa and Hefei varies in the range of 50–150 K depending on the size of the pool fire. A higher flame temperature was also found in Lhasa by Li et al. [9]. In Li's work, the reasons for this were considered to lie in both the reduced flow of air into and thermal radiation loss from the flame at higher altitude. Because the mechanism underlying this phenomenon is very complex, further detailed investigation combining chemical reaction kinetics and flame movement dynamics in low air pressure are required to fully explain it.

The maximum flame temperature, defined as $T_{f(\mathrm{m})}$, is an important parameter of pool fires, significantly influencing their buoyancy and puffing movement.

4.1.2. Mass burning rate

The mass burning rate $\dot{m}''$ of a pool fire is mainly determined by the heat transfer from the flame to the fuel surface. Heat transfer includes the three components of conduction, convection and radiation, which correspond to the three terms as expressed in Eq. (4) [17].

$$\dot{m}'' \propto 4\frac{\lambda(T_f - T_l)}{D} + h(T_f - T_l) + \sigma(T_f^4 - T_l^4)(1 - \exp(-\kappa_s D)) \qquad (4)$$

where T_f is the flame temperature near the burner surface. Previous studies [12,13] investigated the overall trends for the change in regression rate U_l of several fuels with burner size. The regression rate is expressed by $U_l = \dot{m}''/\rho_l$. They found that, conduction from the flame to the burner rim is dominant for pool diameters less than 7 cm. A "transition" from conduction dominated to convection dominated for pool diameters around 7–10 cm. Then burning rates remain roughly constant in the convection dominated region for pool diameters between 10 cm and 20 cm. Then the burning rates steadily increase for diameters increasing from 20 cm to 100 cm due to increasing flame radiation. Finally the burning rate tends to level off for larger diameters.

The rates of regression of the liquid surfaces of ethanol and *n*-heptane in Lhasa and Hefei are shown in Fig. 3a. The air pressure has little effect upon liquid density, so the burning rates exhibit the same trends in their regression rates. In Fig. 3a, the overall trends in the regression rate with burner size are reflected by previous results of Hottel et al. [12,13] .

To further understand air pressure effects upon burning rate, Fig. 3b expresses the variations of the exponent *n*, which describes the dependence of burning rate upon the air pressure as $\dot{m}''_{\mathrm{Lhasa}}/\dot{m}''_{\mathrm{Hefei}} = (p_{\mathrm{Lhasa}}/p_{\mathrm{Hefei}})^n$.

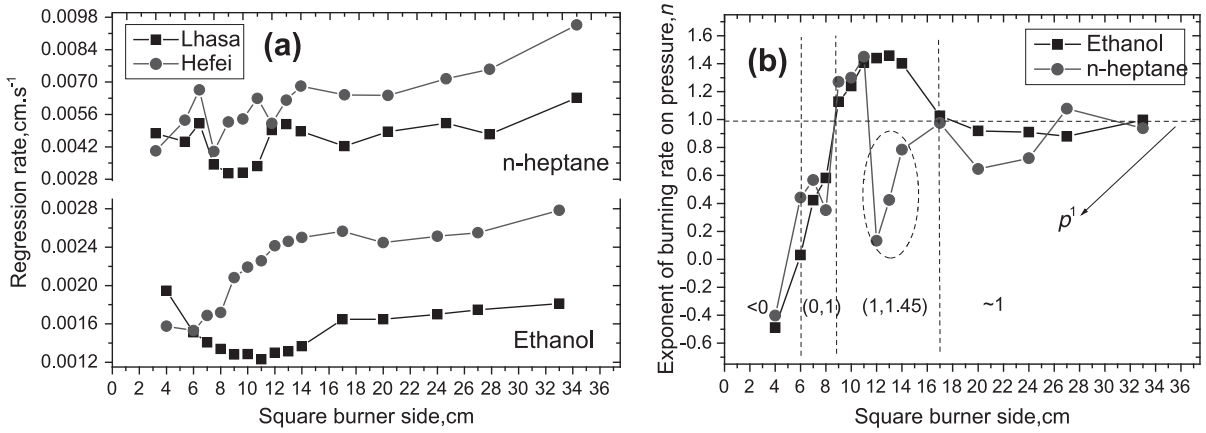

Fig. 3. Regression rates of ethanol and *n*-heptane pool fires (a) in Lhasa and Hefei, and dependence of burning rate exponent on air pressure for ethanol and *n*-heptane pool fires (b).

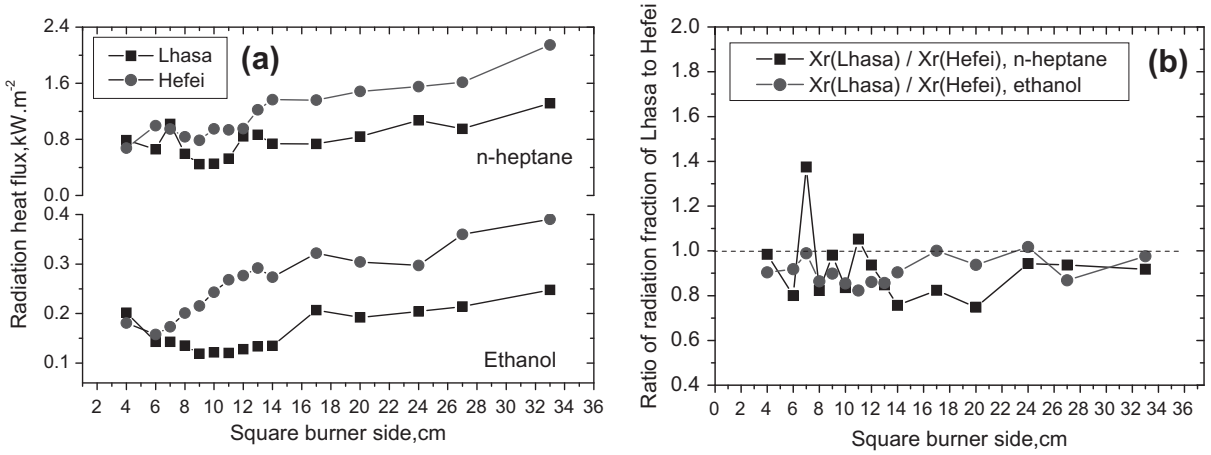

Fig. 4. Radiation heat flux of ethanol and *n*-heptane pool fires: (a) in Lhasa and Hefei, and ratios of radiation fraction, and (b) for Lhasa to Hefei for *n*-heptane and ethanol pool fires.

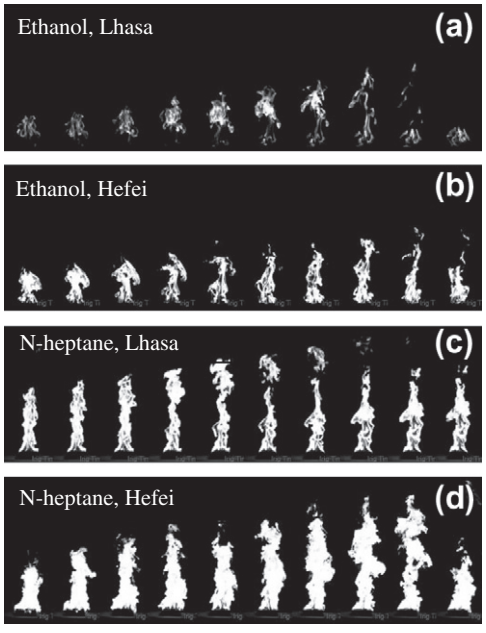

Fig. 5. Sequential flame images in a cycle of flickering movements for ethanol and *n*-heptane pool fires with burner sides of 20 cm.

A new phenomenon is found that, Fig. 3b indicates that low air pressure has different effects upon the burning rates of the pool fires of different sizes. Relating to air pressure effects, Fig. 2 indicates that for very small pool fires with sides of 4 cm, T_f is higher, while Table 1 shows the boiling point T_l of the liquid is smaller in Lhasa. As a result shown in Eq. (4), for pool fires with sides of 4 cm, $\dot{m}''$ is bigger in Lhasa than in Hefei, and n is negative. As the burner size increases, the T_f of pool fires with large sides is lower in Lhasa than in Hefei, so $\dot{m}''$ is smaller in Lhasa. As the burner size increases, the effects of air pressure upon pool fire burning rates vary as different heat transfer mechanisms dominate. As Fig. 3b shows, as the burner size increases, the exponent n starts at a negative value, then increases and becomes positive, until reaches its peak value, then it decreases and finally approaches 1. For a burning rate that is dominated by convection and radiation feedback, theoretical and experimental studies have reported that n is between 0.66 and 1.3 [9,10,18,19].

So, based on the exponent n, four regions can be found for describing the dependence of air pressure upon the fire burning rate with burner size, as summarized in Fig. 3b. A diameter of 10 cm is the turning point for $n = 1$. It is noteworthy that for *n*-heptane fires with 12, 13 and 14 cm sides, there are exceptional variations in n. This is caused by vigorous, fully developed combustion due to ample oxygen at normal air pressure in Hefei.

4.1.3. Flame radiation

Fig. 4a shows the radiation heat flux of ethanol and *n*-heptane pool fires in Lhasa and Hefei. The *n*-heptane pool fires obviously have a higher radiation intensity of heat release than the ethanol ones, but the trends for the change in radiation of the two kinds of fires are similar to their individual regression rates. The radiation fraction of the heat release rate and the specific value for Lhasa to Hefei are described by the following equations:

$$\chi_r = \frac{\dot{Q}_r}{\dot{Q}} = \frac{S_r \cdot \dot{q}_r''}{\dot{m}'' \cdot A \cdot \Delta H_c} \tag{5}$$

$$\chi_{r(\text{Lhasa})}/\chi_{r(\text{Hefei})} = (\frac{\dot{q}_r''}{\dot{m}''})_{\text{Lhasa}}/(\frac{\dot{q}_r''}{\dot{m}''})_{\text{Hefei}} \tag{6}$$

Fig. 4b shows the ratio of radiation fraction for Lhasa to Hefei for *n*-heptane and ethanol fires. In Lhasa, χ_r is generally smaller than in Hefei, which results from the decreased soot formation at low air pressure [8,9]. Supposing that the convection fraction plus the radiation fraction is the same in both locations, the convection fraction in Lhasa is then comparatively larger than that in Hefei.

Combining the observations of the higher axial flame temperature and bigger convection fraction in Lhasa, it is seen that the flame buoyancy in Lhasa is stronger than that in Hefei.

4.2. Effects upon flame oscillation frequency

Fig. 5 shows time-sequence flame images of ethanol and *n*-heptane fires with sides of 20 cm, revealing the periodic puffing movements in Lhasa and Hefei. The pool fire in Lhasa looks narrower and dimmer than that in Hefei, indicating its smaller height and width, and reduced amount of radiation.

Using a fast Fourier transform method, the oscillation frequency was obtained from the variable area of the time-sequenced visible flame images, as shown in Fig. 6(a and b). Fig. 6a compares the flame oscillation frequency of pool fires using the same material in Lhasa and Hefei, while Fig. 6b compares the frequency of pool fires using different fuels in the same place. It can be seen that, for a fire with the same material and burner size, the puffing frequency in Lhasa is greater than that in Hefei. Under the same air

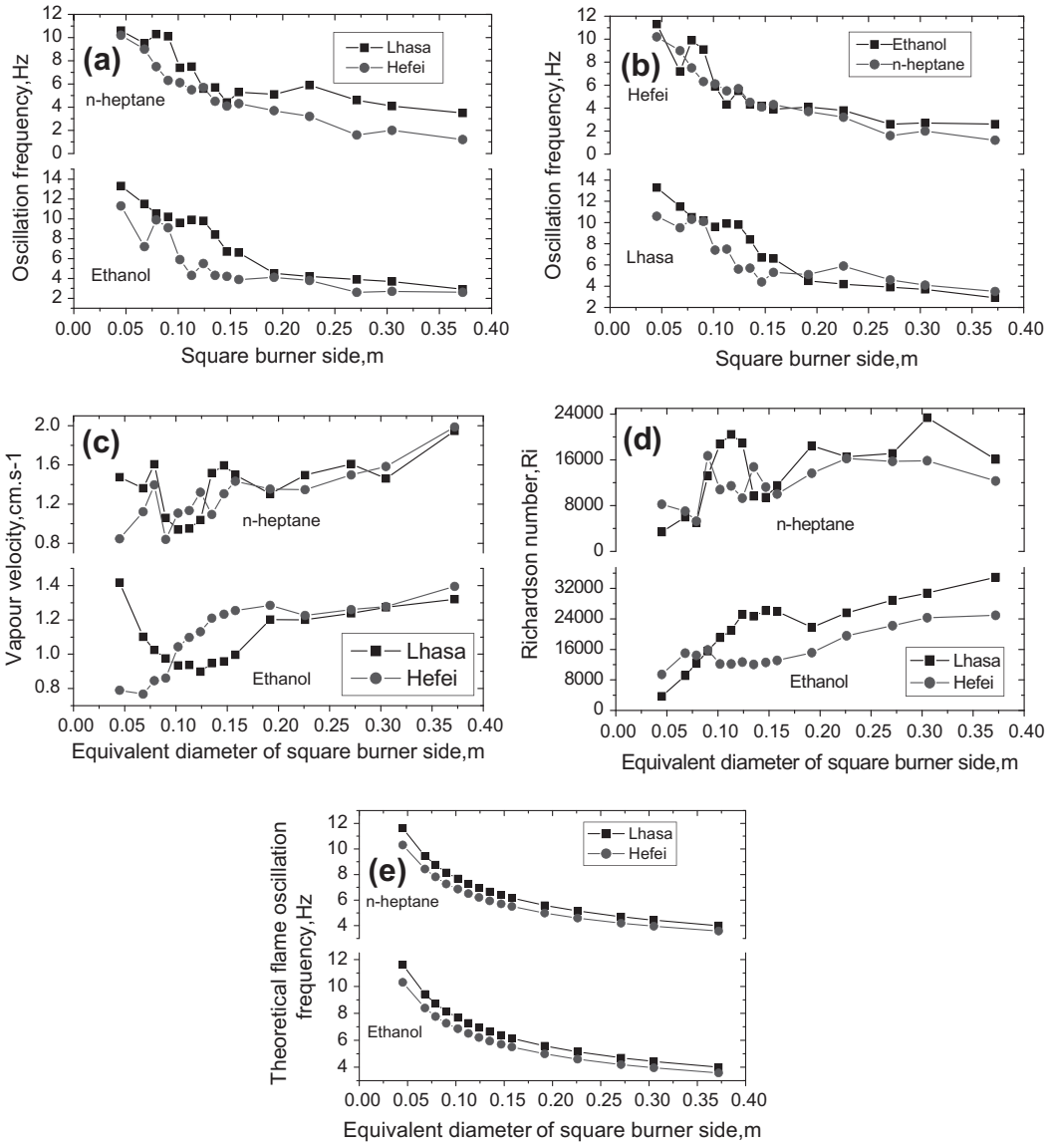

Fig. 6. Experimental puffing frequencies of pool fires: (a) made of the same material in Lhasa and Hefei and (b) composed of ethanol or *n*-heptane in the same place. Vapor velocity (c), Richardson number (d), and theoretical oscillation frequency (e) for ethanol and *n*-heptane pool fires in Lhasa and Hefei.

pressure conditions, the puffing frequency is independent of the fire material, and mainly depends on the burner size.

The above analysis shows that in Lhasa the flame gas temperature is higher and natural convection is stronger, which leads to a larger natural buoyancy. The hot mixing gases in the flame and ambient air should have the same molar mass, so Ri can be rewritten as $Ri = (T_f - T_\infty)gD/(T_\infty U_{f0}^2)$. The approximate average flame temperature $T_{f\ (m)}$ of ethanol and n-heptane fires in Hefei is 700 K, while in Lhasa $T_{f\ (m)}$ is 800 K, and T_∞ is 300 K in Hefei and Lhasa. U_{f0} is the surface-averaged vapor velocity, which is expressed as Eq. (7).

$$U_{f0} = (\rho_l/\rho_{f0}) \cdot U_l \tag{7}$$

Substituting U_{f0} into Ri, F_r, and Eq. (2), and assuming that C is 0.6 [1], U_{f0}, Ri, and the theoretical oscillation frequency can be obtained as depicted in Fig. 6(c–e).

Fig. 6d shows that, except for the smallest pool fire, the Ri of ethanol and n-heptane fires in Lhasa is generally bigger than that in Hefei, indicating fire flames in Lhasa are more buoyant. Fig. 6e indicates that the theoretical oscillation frequency for the same size pool fire in Lhasa is also generally bigger than that in Hefei. Furthermore, the theoretical oscillation frequency is independent of fuel material, which agrees well with the experimental results.

Eq. (3) can be further simplified to Eq. (8) as R_i is very large in the experiments.

$$f = C\sqrt{g}\sqrt{\frac{T_f - T_\infty}{T_\infty}}\frac{1}{\sqrt{D}} \tag{8}$$

Eq. (8) indicates that the puffing frequency is mainly determined by the pool size and the flame buoyancy. In Lhasa, for all burners, $T_{f(m)}$ is higher than in Hefei, so f in Lhasa is bigger than in Hefei.

Cetegen and Ahmed [1] showed that the puffing frequency is closely connected to convection within the height of one diameter above the source of a pool fire. In our experiments, the height with the maximum temperature value is similar to the length of the edge of the square burner, so in Lhasa, the higher maximum temperature produces stronger convection, which leads to a higher puffing frequency.

It has been reported that the puffing frequency decreases in low air pressure [7], which conflicts with the results of our investigation. The main reasons for this discrepancy are that, in the previous research, generally only the air pressure was changed while the air supply was provided with no change in the oxygen density [6–8]. But in Lhasa, both the air pressure and oxygen density decrease, resulting in smaller flame height and width, and less soot formation [9]. In Lhasa, the maximum flame temperature and natural convection increase abnormally and the buoyancy is comparatively strong, leading to a higher puffing frequency.

5. Conclusions

In fire laboratories in Lhasa and Hefei, 15 pool fires of various size were burnt to study the effects of air pressure upon the puffing frequency of the fire. The experimental results show that for the same burner size, the oscillation frequency in Lhasa is bigger than that in Hefei, which results from the higher buoyancy of the flame, verified by the observations of higher flame temperature and smaller radiation fraction in Lhasa. The measured frequency values agree well with the results obtained from theoretical analysis using an empirical equation incorporating the Richardson number, vapor velocity and burner diameter. Furthermore, although the air pressure has a different effect upon burning rate depending on the burner size, for the same air pressure conditions, the puffing frequency is independent of the fuel, and burning rate, and mainly depends on the size of the burner.

Acknowledgements

This work was sponsored by the National Natural Science Foundation of China (Grant No. 51036007). Fang Jun was supported by the National Natural Science Foundation of China (Grant No. 51074147) and Chinese Universities Scientific Fund.

References

[1] Cetegen BM, Ahmed TA. Experiments on the periodic instability of buoyant plumes and pool fires. J Combust Flame 1993;93:157–84.
[2] Malalasekera WMG, Versteeg HK, Gilchrist K. A review of research and an experimental study on the pulsation of buoyant diffusion flames and pool fires. J Fire Mater 1996;20(6):261–71.
[3] Bento DS, Thomson KA, Gulder OL. Soot formation and temperature field structure in laminar propane–air diffusion flames at elevated pressures. J Combust Flame 2006;145:765–78.
[4] Glassman I. Sooting laminar diffusion flames: effect of dilution, additives, pressure, and microgravity. Proc Combust Inst 1998:1589–96.
[5] Liu F, Thomson KA, Guo H, Smallwood GJ. Numerical and experimental study of an axisymmetric coflow laminar methane–air diffusion flame at pressures between 5 and 40 atmospheres. J Combust Flame 2006;146:456–71.
[6] Darabkhani HG, Bassi J, Huang HW, Zhang Y. Fuel effects on diffusion flames at elevated pressures. J Fuel 2009;88(2):264–71.
[7] Durox D, Yuan T, Villermaux E. The effect of buoyancy on flickering in diffusion flames. J Combust Sci Technol 1997;124:277–94.
[8] Most JM, Mandin P, Chen J, Joulain P, Durox D, Fernandez-Pello AC. Influence of gravity and pressure on pool fire type diffusion flames. Proc Combust Inst 1996:1311–7.
[9] Li ZH, He YP, Zhang H, Wang J. Combustion characteristics of n-heptane and wood crib fires at different altitudes. Proc Combust Inst 2009:2481–8.
[10] Fang J, Yu CY, Tu R, Qiao LF, Zhang YM, Wang JJ. The influence of low atmospheric pressure on carbon monoxide of n-heptane pool fires. J Hazard Mater 2008;154:476–83.
[11] International Organization for Standardization. Draft international standard ISO/DIS 7240-15, fire detection and alarm systems. Part 15. Point-type multisensor (light and heat) fire detectors; 2002.
[12] Hottel HC. Certain laws governing the diffusive burning of liquids. Fire Res Abs Rev 1959;1:41.
[13] Blinov VI, Khudiakov GN. Diffusive burning of liquids; 1961 [English translation by US Army Engineering Research and Development Laboratories, T-1490a-c.ASTIA, AD 296762].
[14] Luo M. Effects of radiation on temperature measurement in a fire environment. J Fire Sci 1997;15(6):443–61.
[15] Brohez S et al. A two-thermocouples probe for radiation corrections of measured temperatures in compartment fires. Fire Safe J 2004;39:399–411.
[16] McCaffrey BJ. Purely buoyant diffusion flames: some experimental results. National Bureau of Standards, NBSIR 79-1910; 1979.
[17] Drysdale D. An introduction to fire dynamics. 2nd ed. Chichester: John Wiley and Sons; 1998.
[18] Wieser D, Jauch P, Willi U. The influence of high altitude on fire detector test fires. Fire Safe J 1997;29:195–204.
[19] Alpert RL. Pressure modeling of fires controlled by radiation. Proc Combust Inst 1976:1489–500.